U.S. DEPARTMENT OF COMMERCE
National Technical Information Service

AD-603 487

THE EFFECT OF METAL PROPERTIES ON HYPERVELOCITY PENETRATION

The Johns Hopkins University
Baltimore, MD

Jul 64

THE JOHNS HOPKINS UNIVERSITY

DEPARTMENT OF MECHANICS

77p
hc - 5.00
mf - 0.75

THE EFFECT OF METAL PROPERTIES ON HYPERVELOCITY PENETRATION

(Summary Report)

by

Carroll Mobley
A. M. Dietrich
Eleanor Harrison
Robert B. Pond

Summary Report Prepared for
Ballistics Research Laboratories
Aberdeen Proving Ground
U. S. Army Contract Number
DA-36-034-ORD-3565RD

JULY 1964

Baltimore, Maryland 21218

AD 603 487

THE EFFECT OF METAL PROPERTIES ON HYPERVELOCITY PENETRATION

(Summary Report)

by

Carroll Mobley

A. M. Dietrich

Eleanor Harrison

Robert B. Pond

The Johns Hopkins University

July 1964

Summary Report Prepared for
Ballistics Research Laboratories
Aberdeen Proving Ground
U. S. Army Contract Number
DA-36-034-ORD-3565RD

ABSTRACT

The effect of metal properties on hypervelocity penetration was investigated through the development of energy balances on three target materials, tough pitch copper, 2S Al and mild steel. The effects of such parameters as kinetic energy of impact, orientation of projectile relative to target, geometry of target and prior deformation before hypervelocity penetration were examined through the calculated energy balances. Conclusions were drawn concerning the relation of metal strength parameters and hypervelocity penetration.

INTRODUCTION

During the course of the current investigations on the effect of metal properties on hypervelocity penetration a basic idea of effecting an energy balance was carried out successfully. The problems encountered in developing this energy balance have lead to an array of investigations, some of which have been successfully completed and others of which have been investigated only far enough to delineate the magnitude of the problem involved.

This summary report is designed to show the progress made to date in pursuit of the original concept, as well as to delineate the total problem as it is now understood.

For this reason this report is divided into eleven sections which are titled as follows:

1. Method of Performing Energy Balances
2. The Use of Hardness Measurements in the Determination of Energy Balances
3. The Relation of Energy Balances to Projectile Orientation
4. Energy Balances on 2S Al Air Gun Targets
5. Energy Balances on 2S Al Windowed Targets
6. Energy Balances on 2S Al Pre-Strained Targets
7. Nomographic Method of Energy Balance
8. Energy Balances on Statically Deformed Targets
9. Static Energy Balances on Standard Tensile Specimens
10. Strength Parameters Related to the Partition of Energy
11. General Discussion

METHOD OF PERFORMING ENERGY BALANCES

An earlier paper (1) described a method of performing energy balances for targets penetrated at hypervelocity. This method employed the establishment of a dynamic mechanical energy for a material and its subsequent use to define the partition of impact kinetic energy in variously deformed regions of the target such as the crater or the strain affected region.

The mechanical energy equivalent is generated by establishment of a static true stress-true strain curve for the target and pellet materials. This technique and the underlying hypotheses are described by (2). Some parts of the mathematical and experimental analysis of the targets have been improved and these changes are discussed in sections of this paper. These changes are a) the use of hardness measurements instead of grain growth to delineate the strain gradient below the crater and b) the evaluation of a simpler function to give the energy of the strain affected region. However, the postulates under which the energy balances reported herein are accomplished remain as previously expressed (1). The energy balance is expressed by:

Energy of Impact = Crater Energy + Strain Field Energy + Lip Energy + Projectile Breakup Energy

The strain field energy is expressed by:

$$E_{AR} = \frac{2\pi\sigma_M}{\alpha}\left[\epsilon_m\left\{\left(r_o+\frac{1}{\alpha^2}\right)+\frac{1}{\alpha^2}\right\} - \epsilon_o\left\{\left(r_M+\frac{1}{\alpha}\right)^2+\frac{1}{\alpha^2}\right\}\right] + \frac{2\pi\sigma_m h}{\alpha}\left[\epsilon_m\left(r_o+\frac{1}{\alpha}\right) - \epsilon_o\left(r_M+\frac{1}{\alpha}\right)\right]$$

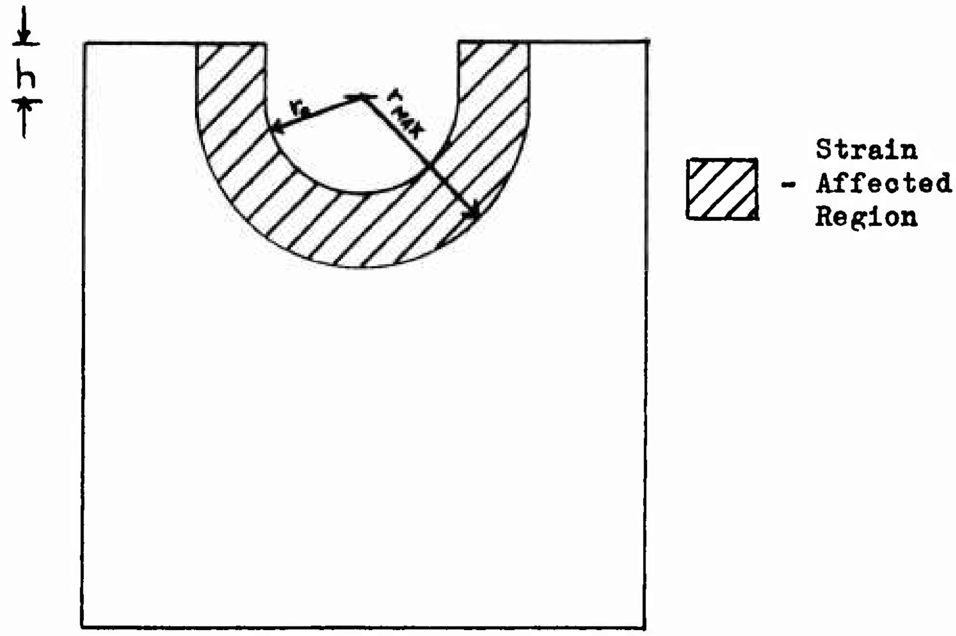

Sketch of Target Cross Section

A summary of values for the targets on which energy balances have been performed is found in Table 1. A plot showing the spread in energy balances for 2S Al, Cu and mild steel is shown in Fig. 1.

Table 2 summarizes the heat treatments given to the targets prior to penetration.

DEFINITION OF TERMS

r_o = crater radius

r_m = radius of affected region

h = height of cylindrical portion of crater

V_o = crater volume

σ_m = rupture stress defined by hypervelocity curve

ϵ_o = strain at r_m } defined by observation of grain

ϵ_m = strain at r_o } growth or hardness measurements

α = constant in $\epsilon = e^{-\alpha(r-C)}$

C = constant in $\epsilon = e^{-\alpha(r-C)}$

E_c = energy of crater formation

E_{AR} = energy of affected region

ϕ = angle between projectile and target

E_T = total calculated energy

E_I = kinetic energy of impact

TABLE 1

Target No.	Impact Velocity (km/sec)	E_I (Joules)	r_o (cm)	r_m (cm)	ϵ_o (in/in)	ϵ_m (in/in)	α (cm^{-1})	h (cm)	V_c (cm^3)	E_c (Joules)	E_{AR} (Joules)	E_T (Joules)	ϕ
Tough Pitch Copper													
1	4.675	1967	0.78	2.26	.045	.556	1.67	0.00	0.95	191	1156	1441	41°
2	4.678	1970	0.84	2.54	.045	.556	1.47	0.00	1.08	215	1581	1888	69°
3	4.827	2097	0.99	2.72	.045	.556	1.66	0.00	1.75	349	1707	2146	90°
4	4.517	1836	0.84	2.54	.045	.556	1.47	0.00	1.40	279	1576	1947	90°
5	4.623	1923	0.86	2.54	.045	.556	1.48	0.00	1.35	270	1568	1927	61°
6	4.694	1983	0.78	2.63	.045	.556	1.43	0.00	0.84	168	1628	1887	29°

$\sigma_m = 5.195 \times 10^4$ psi for all Cu Targets

Target No.	Impact Velocity (km/sec)	E_I (Joules)	r_o (cm)	r_m (cm)	ϵ_o (in/in)	ϵ_m (in/in)	α (cm^{-1})	h (cm)	V_c (cm^3)	E_o (Joules)	E_{AR} (Joules)	E_T (Joules)	ϕ
							2S Al Targets						
1	4.747	2028	1.10	1.90	.075	.735	2.85 2.28	.20	3.41	491	669 1026	1190 1516	16°
2	4.660	1954	1.00	2.25	.075	.735	1.82	1.00	5.03	708	1511	2219	90°
5	4.602	1906	1.10	2.30	.075	.735	1.90	.50	4.61	670	1323	1993	82°
6	4.577	1885	1.10	2.25	.075	.735	1.98	.60	5.02	717	1332	2049	90°
7	4.768	2046	1.10	2.20	.075	.735	2.07 1.90	.30	4.05	584	1085 1288	1669 1872	90°
9	4.592	1898	1.10	2.00	.075	.735	2.85	.10	4.15	586	782	1368	58°
10	4.604	1908	1.00	2.10	.075	.735	2.07	.50	3.59	515	1025	1540	50°
12	3.809	3047	1.05	2.50	.075	.735	1.54	1.25	7.18	1001	2118	3150	83°
14	3.815	3056	1.10	2.45	.075	.735	1.66	1.15	6.51	907	2174	3104	82°
16	3.877	3157	1.15	2.45	.075	.735	1.76	1.20	7.68	1071	2145	3198	90°
17	3.800	3032	1.23	2.30	.075	.735	2.07	.75	5.09	719	1476	2209	30°
18	3.834	3087	1.00	2.45	.075	.735	1.54	1.25	6.80	948	2550	3511	69°
19	3.876	3155	.95	2.28	.075	.735	1.68	.75	4.78	666	1516	2188	36°
20	3.830	3080	1.05	2.50	.075	.735	1.54	1.25	7.64	1064	2118	3202	90°

Target No.	Impact Velocity (km/sec)	E_I (Joules)	r_o (cm)	r_m (cm)	ϵ_o (in/in)	ϵ_m (in/in)	α (cm^{-1})	h (cm)	V_o (cm^3)	E_o (Joules)	E_{AR} (Joules)	E_T (Joules)	ϕ
2S Al Pre-Strained Targets													
			1.06	3.73	.001	.508	2.34	0.17	3.271	321	689	1010	
101	4.811	2083	1.06	2.35	.010	.497	3.33	0.17	3.271	314	424	738	-
			1.06	3.12	.001	.497	3.03	0.17	3.271	314	450	764	
102	4.557	1869	1.05	3.57	.001	.788	2.64	0.04	2.784	424	807	1230	-
103	4.877	2141	1.08	2.05	.010	1.38	5.12	-.06	3.121	832	530	1361	48°
104	4.280	1649	.98	2.34	.001	1.41	5.39	.65	4.118	1121	783	1904	-
105	4.706	2003	1.045	3.44	.001	.651	2.711	.24	3.666	461	711	1173	52°
106	4.839	2107	1.03	2.56	.001	.572	4.14	.17	2.775	307.5	325	632	-
107	4.835	2139	1.10	5.58	.001	.380	1.34	0.17	3.685	270	1514	1784	-

Special Analysis of Targets 104 and 105 Referred to in Section 6

	Impact Energy	Estimated Energy of Forging	Total Calculated Energy
104	1649	6765	19,862
105	2003	15200	3,180

σ_m = 2.80×10^4 psi for <u>all</u> 2S Al Targets

Target No.	Impact Velocity (km/sec)	E_I (Joules)	r_o (cm)	r_m (cm)	ϵ_o (in/in)	ϵ_m (in/in)	α (cm^{-1})	h (cm)	V_c (cm^3)	E_o (Joules)	E_{AR} (Joules)	E_T (Joules)	ϕ
23	4.006	9003	1.83 1.85	3.54 3.64	.075	.735	1.33	.33 .35	16.61	2382 2382	3938 4146	6319 6528	32°
37	4.086	9366	1.75 1.75 1.75	3.63 3.00 3.00	.075	.735	1.21 1.82 1.89	.65 .60 .60	15.19	2100 2100 2120	4880 2550 2468	6980 4650 4588	22°
38	3.945	8730	1.65 1.65 1.65 1.65	3.32 2.53 3.50 3.55	.075 .075 .07 .04	.735 .735 .735 .735	1.38 2.60 1.52 1.76	1.00 1.00 1.00 1.00	17.80	2400 2400 3884 4124	4180 1755 6058 5581	6580 4155 9943 9705	42°
2S Al Window Targets													
40	3.02	3639	1.30	4.25	.01	.99	1.57	0.07	5.095	975	3078	4053	12°
41	2.93	3425	1.32	3.87	.01	1.34	1.88	0.11	5.00	1294	3243	4537	16°
45	2.79	3106	1.30 1.26	3.90 3.86	.01 .01	.764 .922	1.73 1.73	0.09 0.09	5.085 5.085	750 750	1998 2363	2749 3268	32°
47	2.76	3039	1.28	3.62	.01	1.38	2.08	0.17	5.55	905	2641	4120	31°
50	2.90	3356	1.28	3.28 3.96	.01 .01	1.05 1.13	2.33 1.73	0.44	5.91	1479	2155 3511	3353 4801	28°

Target No.	Impact Velocity (km/sec)	E_I (Joules)	r_o (cm)	r_m (cm)	ϵ_o (in/in)	ϵ_m (in/in)	α (cm^{-1})	h (cm)	V_c (cm^3)	E_ρ (Joules)	E_{AR} (Joules)	E_T (Joules)	ϕ
1014 Steel													
3	4.6669	1960	0.65	2.15	.001	0.72	4.35	0.00	0.373	199	635	834	3°
			0.68	2.18	.001	0.72	4.38	-0.09	0.380	203	608	811	
			0.68	2.06	.001	1.24	5.15	0.00	0.341	316	855	1171	
			0.68	2.06	.001	1.37	4.83	0.00	0.341	349	1102	1452	
4	4.625	1925	0.65	2.15	.008	0.72	2.99	0.15	0.758	405	1286	1691	72°
			0.71	2.21	.008	0.72	3.00	0.11	0.771	412	1270	1682	
			0.71	2.74	.001	1.35	3.53	0.11	0.743	750	2105	2855	
			0.71	2.76	.001	1.07	3.70	0.11	0.743	595	1674	2269	
5	4.646	1943	0.60	2.15	.004	0.72	3.46	0.20	0.60	320	509	829	52°
			0.66	2.16	.004	0.72	3.49	0.19	0.517	276	748	1024	
			0.66	2.56	.001	0.72	3.46	0.19	0.489	263	813	1076	
			0.66	2.65	.001	0.92	3.58	0.19	0.489	336	918	1254	
6	4.670	1963	0.60	2.10	.003	0.72	3.78	0.20	0.814	435	855	1290	72°
			0.67	2.17	.003	0.72	3.77	0.17	0.826	441	976	1417	
			0.67	2.31	.001	1.05	4.25	0.17	0.775	609	1189	1797	
			0.67	2.31	.001	0.82	4.22	0.17	0.775	475	922	1397	
7	4627	1927	0.70	2.20	.004	0.72	3.46	0.00	0.733	391	851	1242	71°
			0.74	2.24	.004	0.72	3.49	0.01	0.762	407	1078	1485	
			0.74	2.33	.001	1.16	4.45	0.01	0.710	616	1160	1776	
			0.74	2.33	.001	1.09	4.43	0.01	0.710	579	1142	1721	
10	3.880	8445	1.18	2.90	.007	0.72	2.69	0.00	2.455	1317	3051	4368	46°
			1.18	3.39	.001	1.40	2.13	0.00	2.455	2572	9027	11599	
			1.18	3.39	.001	1.73	3.52	0.00	2.455	3177	5119	8296	

Target No.	Impact Velocity (km/sec)	E_I (Joules)	r_o (cm)	r_m (cm)	ϵ_o (in/in)	ϵ_m (in/in)	α (cm^{-1})	h (cm)	V_c (cm^3)	E_c (Joules)	E_{AR} (Joules)	E_T (Joules)	ϕ
11	3.771	7997	1.08	2.88	.007	0.72	2.57	0.05	3.013	1610	2991	4601	63°
			1.08	3.68	.001	0.64	2.48	0.00	3.00	1436	2527	3963	
			1.08	3.68	.001	0.64	2.48	0.05	3.00	1436	2607	4044	
			1.08	3.68	.001	0.73	2.74	0.05	3.00	1629	4304	5933	
12	3.975	8864	1.15	2.55	.001	0.72	3.06	-0.25	2.35	1255	1990	3500	48°
			1.15	3.73	.001	1.20	2.75	0.00	2.337	2097	4940	7038	
			1.15	3.73	.001	1.20	2.75	-0.25	2.337	2097	4182	6279	
			1.15	3.73	.001	1.90	3.23	-0.25	2.337	3321	5119	8439	
13	3.922	8629	1.14	2.89	.004	0.72	2.96	-0.25	2.289	1223	2127	3350	42°
			1.14	3.32	.001	1.00	3.16	0.00	2.273	1688	3259	4947	
			1.14	3.32	.001	1.00	3.16	-0.25	2.273	1700	2741	4441	
			1.14	3.32	.001	1.11	3.44	-0.25	2.273	1887	2678	4565	
14	3.975	8864	1.13	2.90	.007	0.72	2.61	-0.20	2.241	1197	2617	3814	60°
			1.13	2.91	.001	1.20	3.99	0.00	2.231	1978	3806	5784	
			1.13	2.91	.001	1.20	3.99	-0.20	2.231	2003	2372	4375	
			1.13	2.91	.001	1.95	4.23	-0.20	2.231	3254	3687	6941	
16	3.854	8333	1.16	2.98	.005	0.72	2.73	0.10	3.349	1789	3130	4919	68°
			1.16	3.54	.001	0.92	2.87	0.00	3.338	2171	3570	6741	
			1.16	3.54	.001	0.92	2.87	0.10	3.338	2297	3808	6105	
			1.16	3.54	.001	0.77	2.84	0.10	3.338	1933	3234	5167	
17	3.822	8195	1.08	2.70	.006	0.72	2.95	0.50	3.651	1951	4106	6057	90°
			1.08	3.19	.001	0.90	3.23	0.00	3.626	2441	2643	5084	
			1.08	3.19	.001	0.90	3.23	0.50	3.626	2441	3499	5940	
			1.08	3.19	.001	1.04	3.33	0.50	3.626	2820	3843	6663	

$\sigma_m = 1.087 \times 10^5$ psi for all 1014 Steel Targets

Table 2

Summary of Treatment of Targets

Prior to Deformation

Material	Target No.	Heat Treatment
Tough Pitch Copper	1,2,3,4,5,6,7	Packed in graphite, placed in 1400°F furnace and allowed to stabilize to 1400°F. Held 2 hours at 1500°F, then furnace cooled.
2S Al	1 through 26, 31 W through 50W (Window targets - W)	Heated from room temperature to 1100°F; held 1 hour at 1100°F; furnace cool.
1014 Steel	1 through 17	Heated to 1650°F; held 1-3/4 hours at 1700°F. and furnace cooled.
2S Al	101 through 107	No heat treatment. As received stock forged from four inches to three inches.
2024 Al	1 through 8	As received stock

Targets not Analyzed:

Cu - 7

2S Al - 3,4,8,11,13,15,22,24,25, and 26; 31W through 39W, 42,43,44, 46,48,49

1014 Steel - 1,2,8,9,15

Several energy balances were performed on each of the mild steel targets. This was due to an anomaly in the value of rupture strain. The rupture strain, ϵ_m, determined from the dynamic stress-strain curve did not agree with the value derived from hardness measurements.

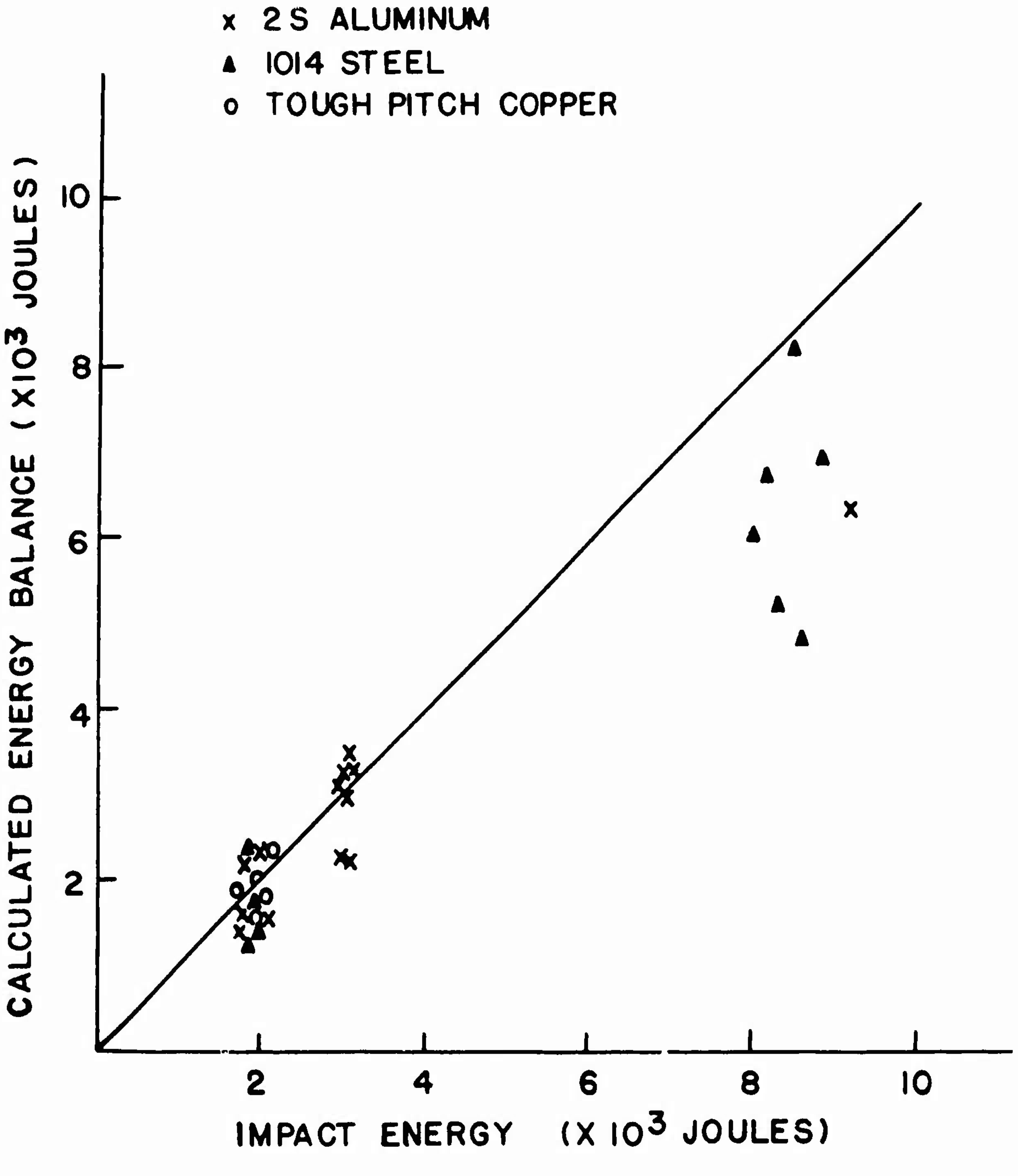

Fig. 1. Comparison of Calculated Energy Balance with Impact Energy for 2S Al, Cu, and 1014 Steel

THE USE OF HARDNESS MEASUREMENTS IN THE DETERMINATION OF ENERGY BALANCES FOR HYPERVELOCITY IMPACT

The "Strain versus Distance from Crater" graphs which were used in the initial energy balances for copper and 2S Al targets (1) were developed from grain size measurements on the individual targets. Grain size, after annealing, as a function of strain was determined from tapered tensile specimens of the two materials. For both graphs, not only was the measurement of the grain sizes tedious, but also the method was insensitive to low strain values (strains below 3%). Thus a parameter more sensitive and, if possible, more easily measurable than grain size was sought in order to develop "Strain versus Distance from Crater" curves for all the materials used as targets. Hardness was thought to be such a parameter since hardness, like grain size after annealing, is a function of deformation energy.

Three methods of measuring hardness were examined for each of the materials used as targets. The three methods were: (1) Vickers microhardness, (2) Rockwell hardness and (3) Width of scratch made with a glasscutter under a constant load. The load was varied for each of the methods in order to determine the most sensitive testing conditions. It was noted after preliminary testing that any one of the hardness methods could be used. Naturally, the best method was desired. Selection of one of these three methods was made in terms of reproducibility, sensitivity, and the number of readings possible per unit length. Reproducibility was determined by taking several readings with each of the methods and comparing the relative amount of scatter between the sets of data. Sensitivity was decided by noting which method was most sensitive to low strains. For the number of readings possible per unit length, the three methods were rated as: (1) Continuous scratch made with the glasscutter, (2) Vickers microhardness, and (3) Rockwell hardness. For a given unit of length on any specimen more readings could be made from the scratch than from the Vickers and more from the Vickers than the Rockwell.

The three methods were compared on copper, 2S Al, 2024 Al, and 1014 Steel. For all four materials it was found that the Vickers microhardness method was the most reproducible and sensitive. The Rockwell was second for all the materials. Therefore, the Vickers microhardness (30 kilogram load) method was adopted as the standard method for measuring hardness on the target materials.

The Vickers hardness measurements were not only reproducible, they were also extremely sensitive to low strain values (being capable of measuring strains as low as 0.1%). Thus, it was possible to obtain "Strain versus Distance from Crater" graphs more accurately than with the grain size method and also to measure the strain in any part on the specimens. Therefore, the energy balances were sharpened in accuracy.

One apparent problem has been noted. The hardness, like the grain size after annealing, appears to be a function of strain rate. Thus, the maximum hardness values on the hypervelocity targets are relatively higher than those on standard tensile specimens. Rate studies are being made in order to determine the correlation between hardness measurements and strain rate. Development of strain vs. distance from crater in 2S Al is given in Figures 2, 3 and 4.

These plots were developed by first determining the variation of Vickers hardness (cross diameter of pyramidal impressions) with strain level on a tapered tensile of target material, Fig. 2. Then a plot of hardness vs. distance from the crater was made (Fig. 3). Finally, by cross plotting the two previous graphs, Fig. 4 is obtained, a plot of strain versus distance from crater. If this plot is made in terms of logarithm of strain vs. r, it is possible to read off values of α and c in $\epsilon = e^{-\alpha(r-c)}$ via the slope and intercept method (Fig. 5).

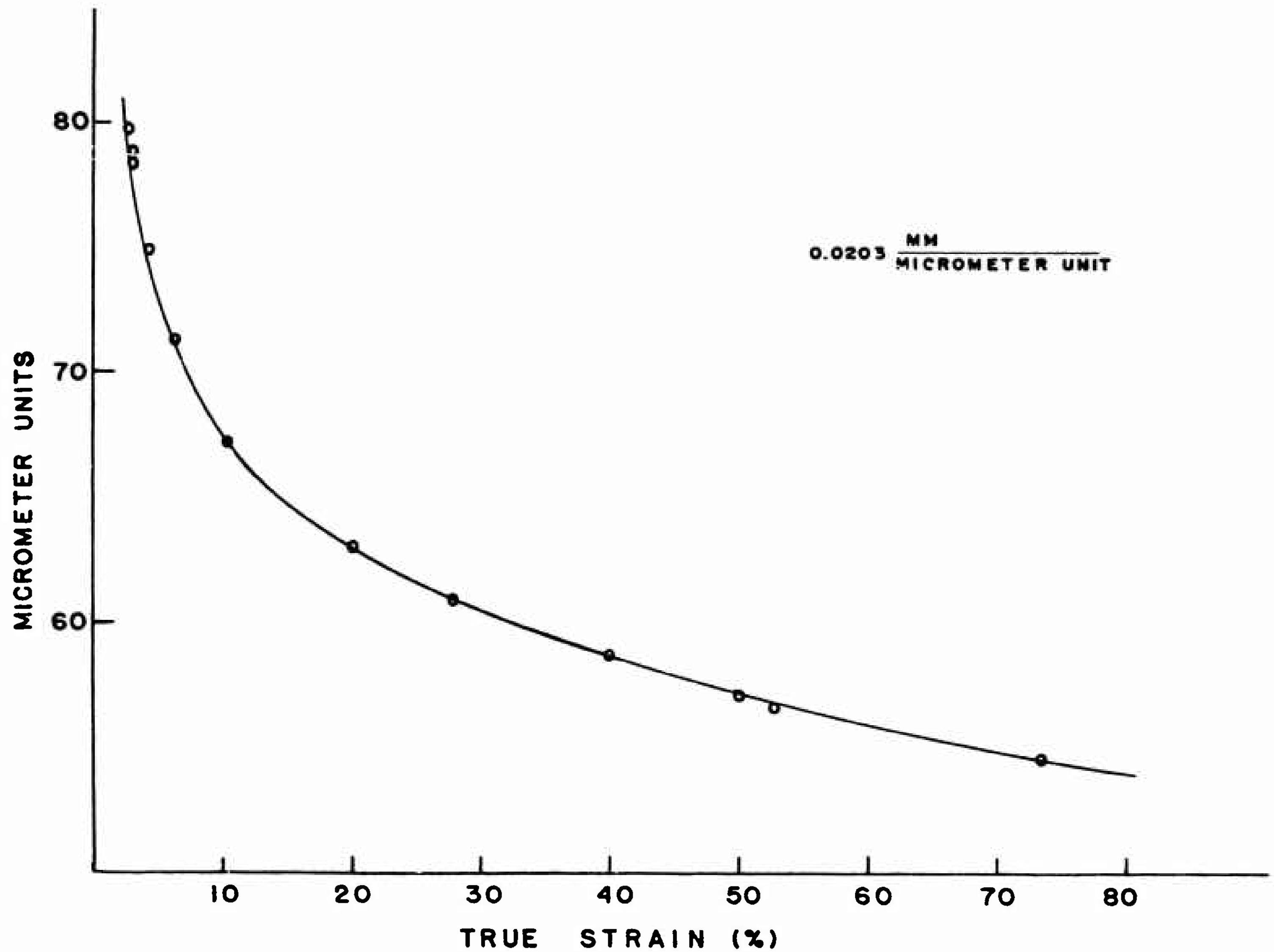

Fig. 2. Average Cross Corner Diameter of Pyramidal Impression vs. Strain
2S Al Tapered Tensile No. 18

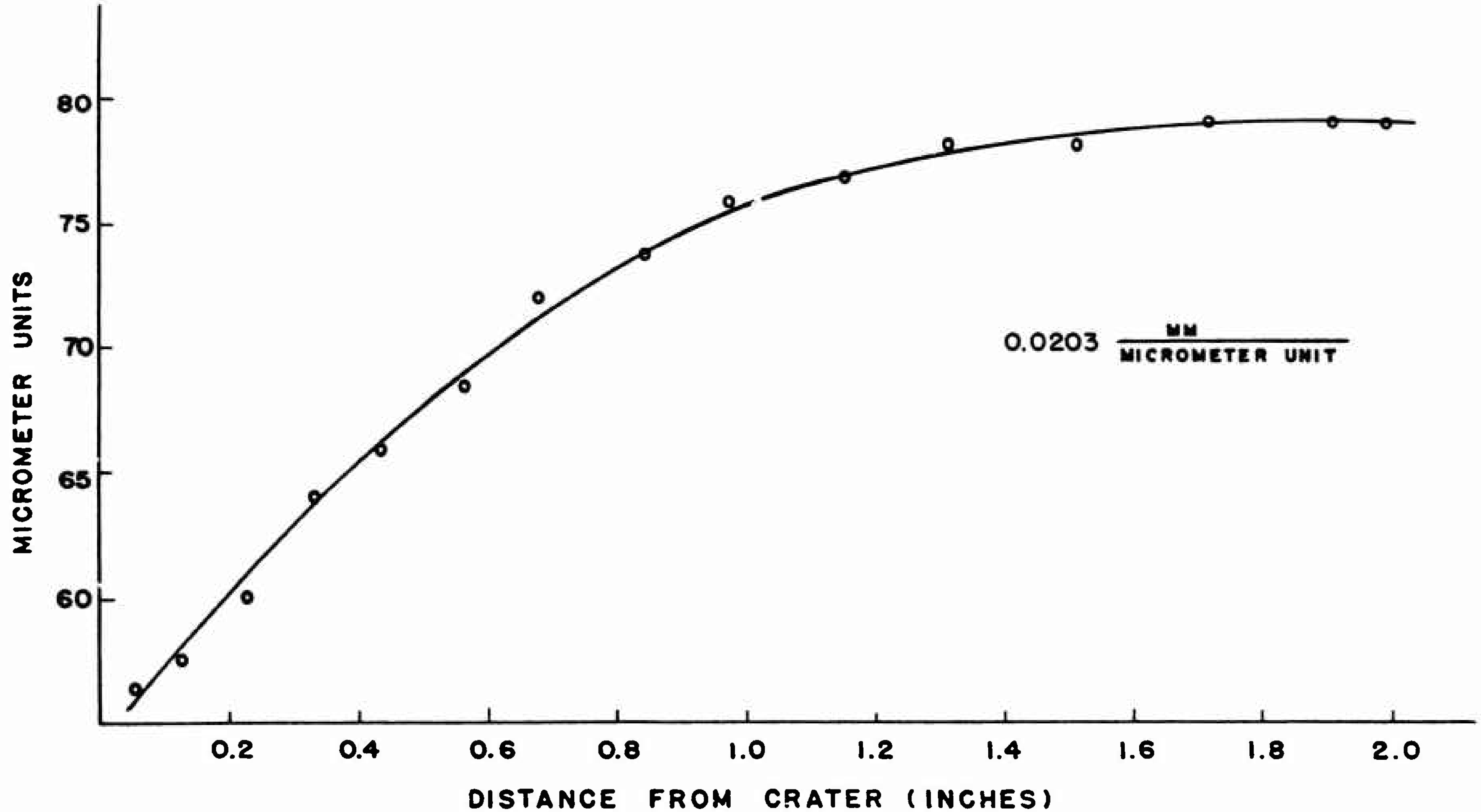

Fig. 3. Cross Corner Diameter of Pyramidal Impression vs. Distance from Crater - 2S Al Target No. 41

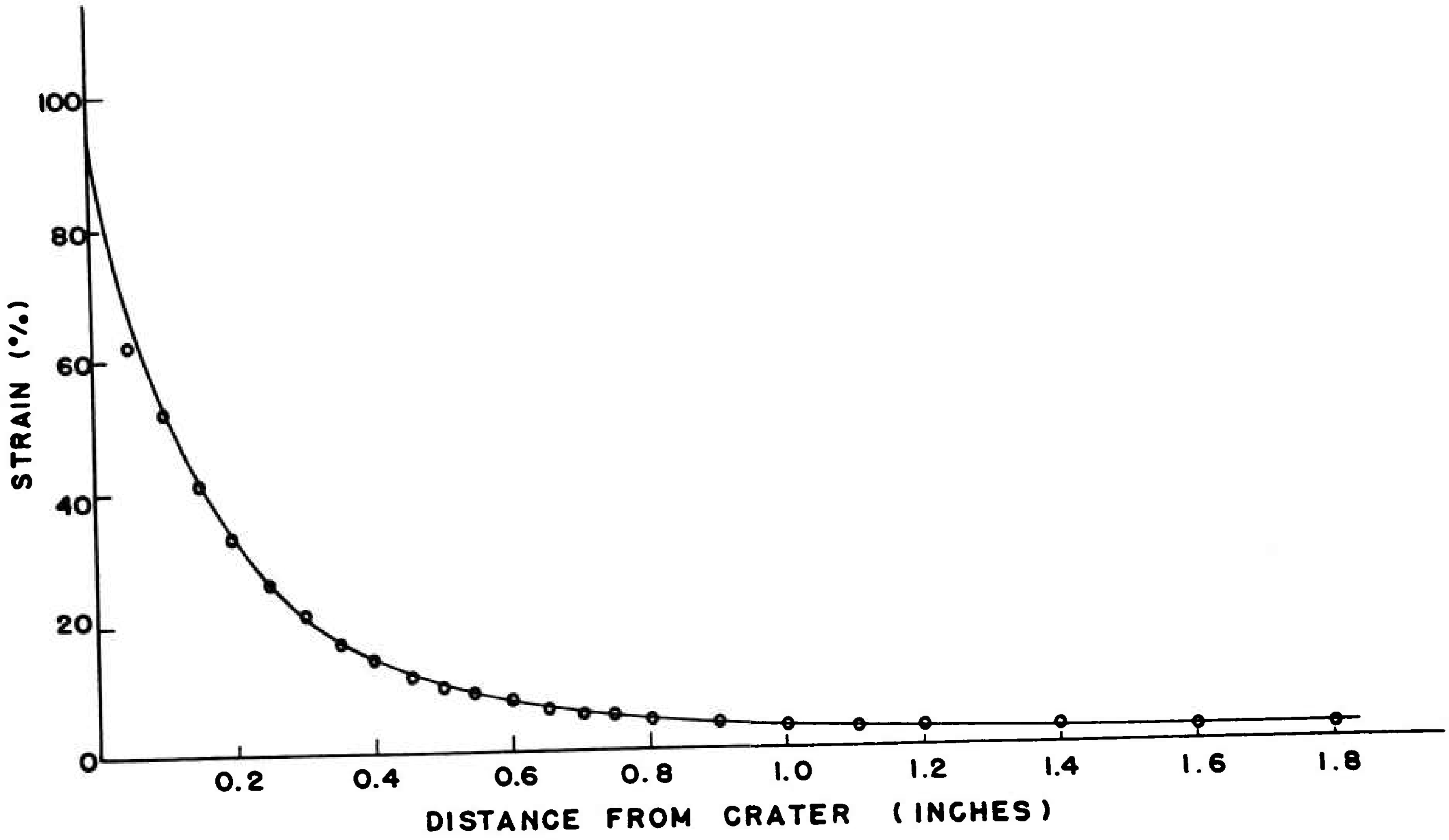

Fig. 4. Strain vs. Distance from Crater 2S Al Target No. 41 W

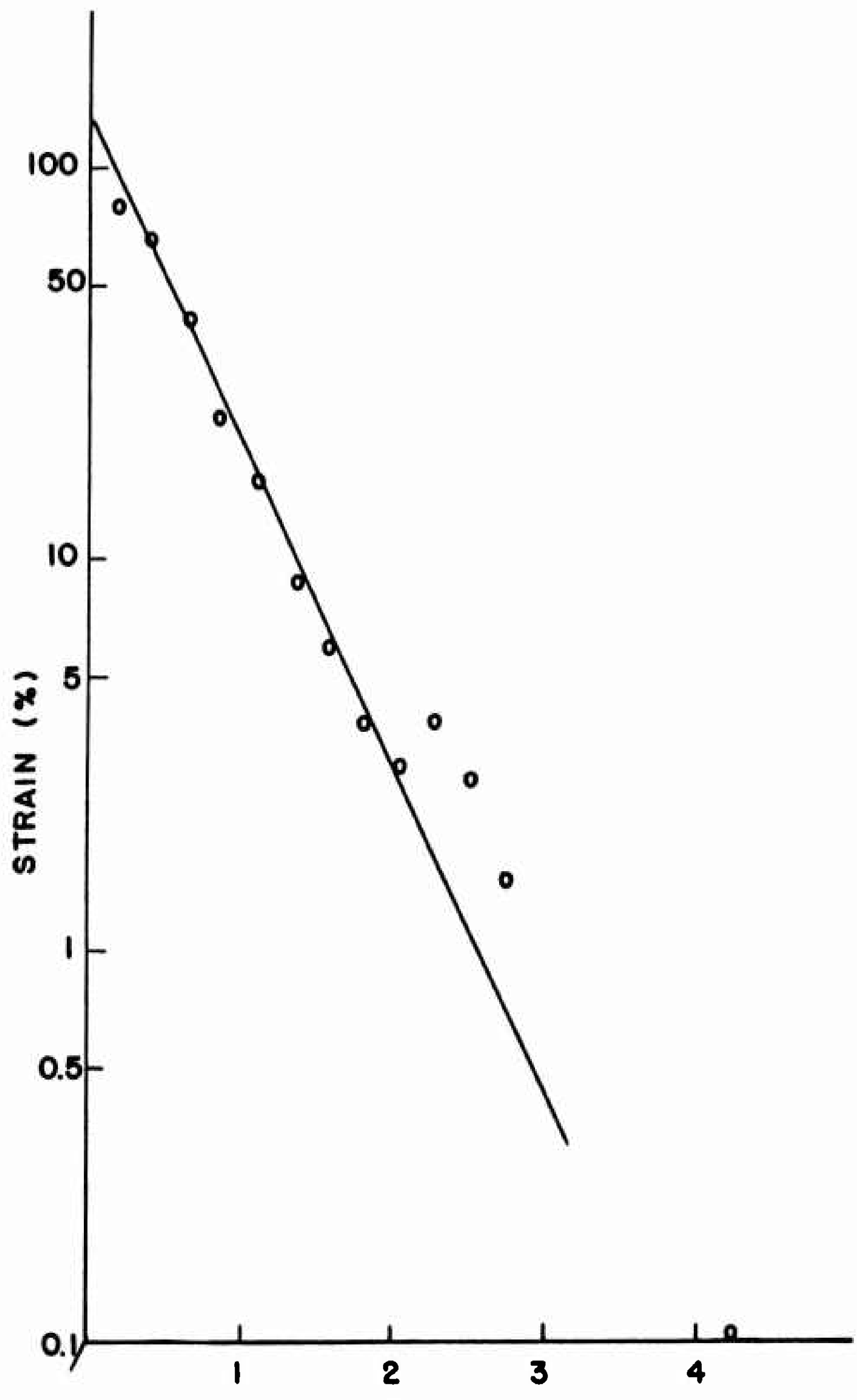

Fig. 5 - Strain vs. Distance from Crater
(Semi-Log)
2S Al Target No. 41 W

THE RELATION OF ENERGY BALANCES TO PROJECTILE ORIENTATION

In examining the results of the energy balances in Cu and 2S Al at 2000-3000 Joules input it was found that some of the balances did not agree with the known impact energy within reasonable limits. Energy balances are initmately dependent upon variables derived from measurements on the targets. An examination of these target variables was necessary to determine whether a systematic change occurred in any of them which was related to the energy balance error. When such a procedure was carried out, the following observations were made:

1) The ratio of the crater volume of a target to the average of all target crater volumes at a fixed impact energy is low whenever the ratio of the energy balance, E_T to the impact energy is low. The term "low" means less than one.

2) The variables r_o and r_m defined earlier in the paper do not vary much at the tested energy levels in aluminum and copper, but the depth of the crater, P_c , has a variation an order of magnitude higher than r_o or r_m (Tables 4 and 5).

3) Projectile orientation is shown to govern this variation in depth, and hence in volume, of the crater; however, only inferences may be made as to the nature of this effect on energy balances in the strain affected region.

In Table 3 the ratios of $\frac{\text{Volume of Crater}}{\text{Avg. Volume of Crater}}$ $(V_c/\bar{V}_c)$ and $\frac{\text{Total Computed Energy}}{\text{Impact Energy}}$ (E_T/E_I) are given for the targets discussed herein. From the plots (Figs. 6,7) of crater volume (V_c) vs. impact energy E_I the mean values of these variables are linear for the velocities tested. Since the projectiles fired into the targets were disc shaped, they could give different effective areas as a source of kinetic energy depending on their angle of tilt relative to the target surface at impingement.

The geometry of the problem is the following: The projectile is a disc. If normals are chosen to the target surface and to the pellet surface, then the cosine of the angle between these normals is proportional to the projected area of the pellet on the target surface. That is, if ϕ is the angle in question, then cos ϕ is a minimum where the projected area is a minimum and is a maximum where the projected area is a maximum.

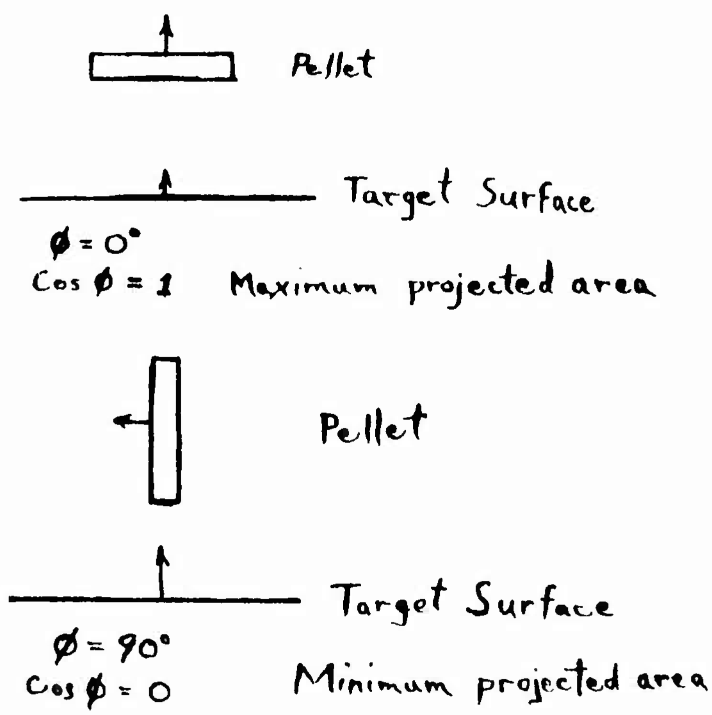

The angle ϕ is measured by stereographic projection using BRL values for two angles of rotation about independent axes.

From plots of crater volume (V_c) vs. cos. ϕ (Fig. 8) at constant energy a linear variation is observed. The minimum volume occurs at $\phi = 0°$ and the maximum volume at $\phi = 90°$. The dispersion of points on these plots is felt to be due in part to a dispersion of energies about the mean for each charge design.

Another source of error is the uncertainty of the pellet orientation because the documentation of the angle is made at some distance from the target surface. To examine this error the maximum tolerable pellet rotation velocity is estimated and compared with the value calculated from BRL's flash sequence on targets 31 - 50. If a pellet translational velocity of 4 - 5 km/sec, a distance at radiograph of 5 cm and a variation in ϕ of 5° are chosen, this corresponds to a maximum tolerable tumble rate of 1100 - 1400 r.p.s. Perusal of the tumble rate values for the aforementioned flash sequence shows that all but one of the values at the radiograph closest to the target are below the maximum allowance. (On the assumption that the pellet does not turn 180° + $\Delta\phi$ or 360° + $\Delta\phi$, etc.)

The estimated error in cos ϕ for a 5° variation in ϕ is then:

$$\Delta(\cos\phi) = \sin\phi \, \Delta\phi$$

$$\text{or} \quad \Delta(\cos\phi) = \pm .088 \text{ for } \Delta\phi = \pm 5° \text{ at } \phi = 90°$$

Unfortunately the charge designs were different at different energies and the effect of pellet area on volume may not be isolated from the effect of energy on volume as a function of pellet orientation. Each line on the plot, Fig. 8, for a material and energy gives only relative effects of projected area.

In terms of the energy balances the effect of pellet orientation is not understood. Mathematically, the greatest energy per unit volume is ascribed to the crater region. Thus, when the crater is small and the maximum extent of the strain affected region has not increased (noting the aforementioned consistency of r_m), the energy balances will obviously be low. Part of the answer in a physical sense may be in the use of the strain gradient function $\epsilon = e^{-\alpha(r-c)}$

This function contains only a radial variation which might be taken to imply deformation proceeding from a point source. A disc projectile striking on its edge is more closely a point source than is the same projectile striking on its face.

Table 3

2S Al			
Target	Cos ϕ	$V_c/\bar{V}_c$	E_T/E_I
1	.961	0.798	0.748
2	.000	-	-
3	.485	-	-
5	.139	1.080	1.045
6	.000	1.176	1.082
7	.000	0.948	0.915
8	.035	-	-
9	.530	0.972	1.020
10	.643	0.842	0.802
12	.122	1.171	1.029
13	.174	-	-
14	.139	1.020	1.016
15	.857	-	-
16	.000	1.204	1.013
17	.866	0.798	0.728
18	.358	1.066	1.137
19	.809	0.749	0.694
20	.000	1.197	1.039
23	.848	-	0.770

Cu			
Target	Cos ϕ	$V_c/\bar{V}_c$	E_T/E_I
1	.755	0.805	0.733
2	.358	0.915	0.954
3	.000	1.48	1.023
4	.000	1.18	1.06
5	.485	1.14	1.00
6	.875	0.712	0.952
7	.995	-	-

Table 4

	Target No.	Penetration (cm)	Diameter Crater (cm)	P_c/D_c	E_T/E_I	Cos Ø
2S Al	1	1.26	2.26	0.56	0.748	0.961
	2	1.85	1.99	0.93	-	0.000
2000 Joules	3	1.53	2.18	0.70	-	0.485
	4	1.41	2.32	0.61	-	-
	5	1.77	2.25	0.79	1.045	0.139
	6	1.73	2.14	0.81	1.082	0.000
	7	1.66	2.17	0.76	0.915	0.000
	8	1.46	2.29	0.74	-	0.035
	9	1.36	2.34	0.58	1.020	0.530
	10	1.29	2.28	0.57	0.802	0.643
	11	1.86	2.38	0.78	-	-
	12	2.35	2.16	1.08	1.029	0.122
3000 Joules	13	2.38	2.04	1.17	-	0.174
	14	2.30	2.15	1.10	1.016	0.139
	15	1.32	2.34	0.56	-	0.857
	16	2.48	2.22	1.12	1.013	0.000
	17	1.64	2.38	0.69	0.728	0.866
	18	2.27	2.04	1.11	1.137	0.358
	19	1.33	2.39	0.56	0.694	0.809
	20	2.28	2.21	1.03	1.039	0.000
9000 Joules	23	2.12	3.82	0.50	0.770	0.848
Cu	2	0.72	2.39	0.30	0.954	0.755
	3	1.09	1.83	0.60	1.023	0.000
	4	0.83	1.75	0.42	1.06	0.000
	5	0.73	1.63	0.45	1.00	0.485
	6	0.73	1.67	0.44	0.952	0.875

Table 5

Target No.	Impact Energy (E_I) Joules	$\bar{r}_o$(cm)	$\bar{r}_{max}$(cm)	$\bar{V}_c(cm)^3$	P_c (cm)
2S Al					
1,5,6,7, 9,10	1948 $\pm$ 53.3	1.12 $\pm$ .023	2.24 $\pm$ .08	4.27 $\pm$ .46	1.57 $\pm$ .226
12,14,16, 17,18,19, 20	3088 $\pm$ 39	1.10 $\pm$ .05	2.40 $\pm$ .044	6.38 $\pm$ 1.05	2.14 $\pm$ .326
23	9003	1.85	2.50	17.09	2.20
Tough Pitch Cu					
1-6	2000	.84 $\pm$ .05	2.54 $\pm$ .09	1.18 $\pm$ .28	.80 $\pm$ .09

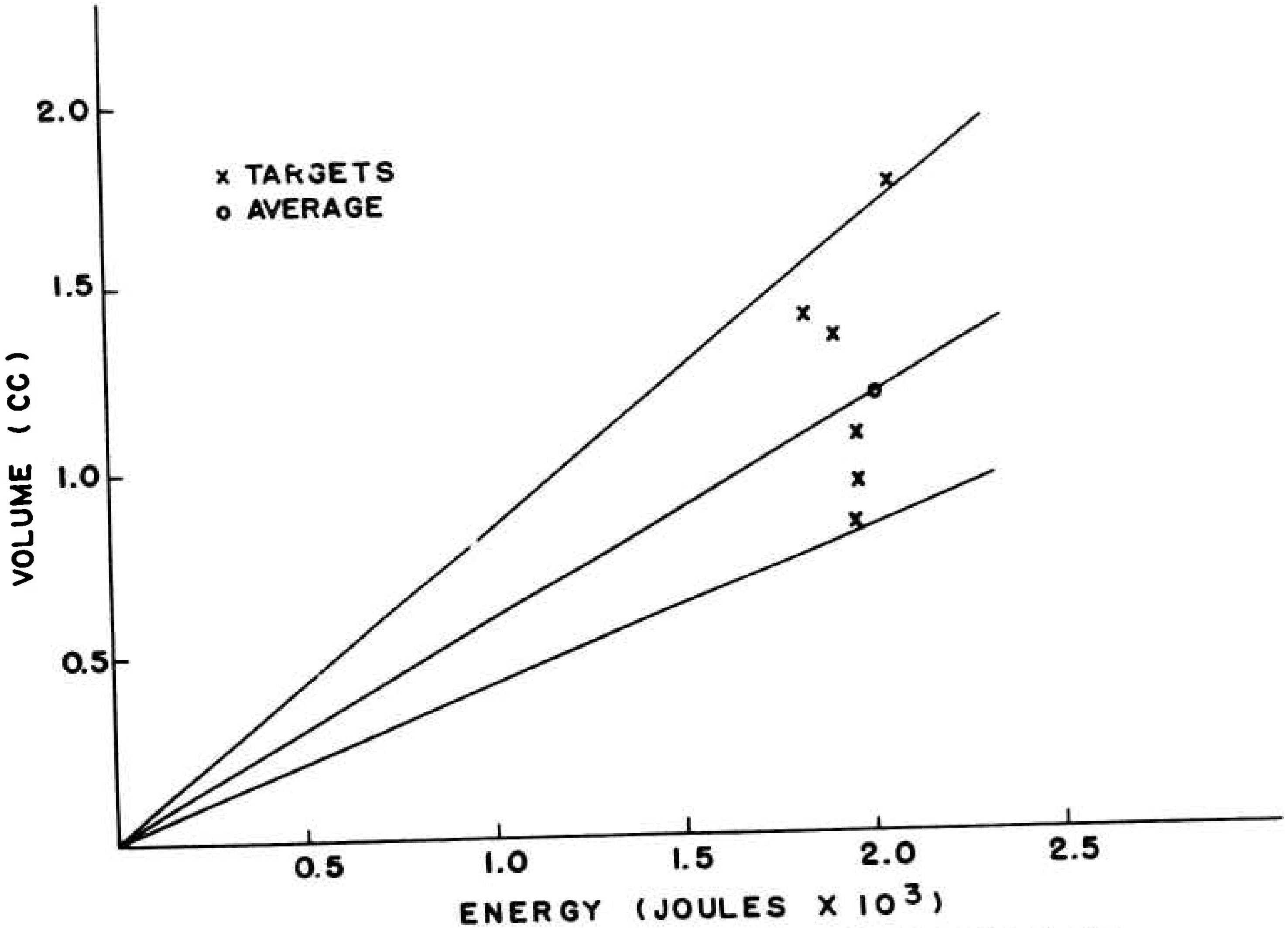

Fig. 6. Crater Volume vs. Impact Energy - Tough Pitch Copper

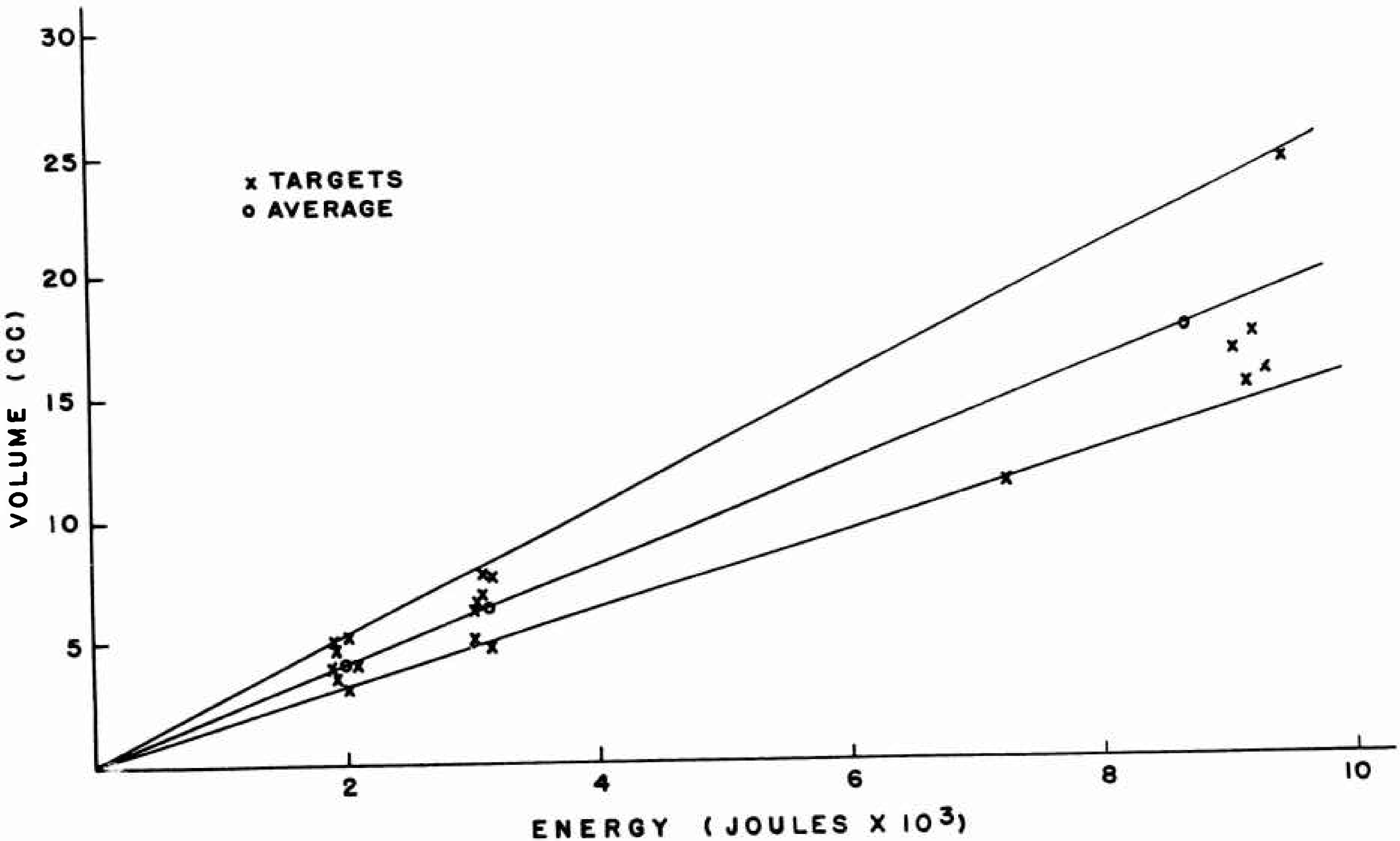

Fig. 7. Volume of Crater vs. Impact Energy
Annealed 2S Al

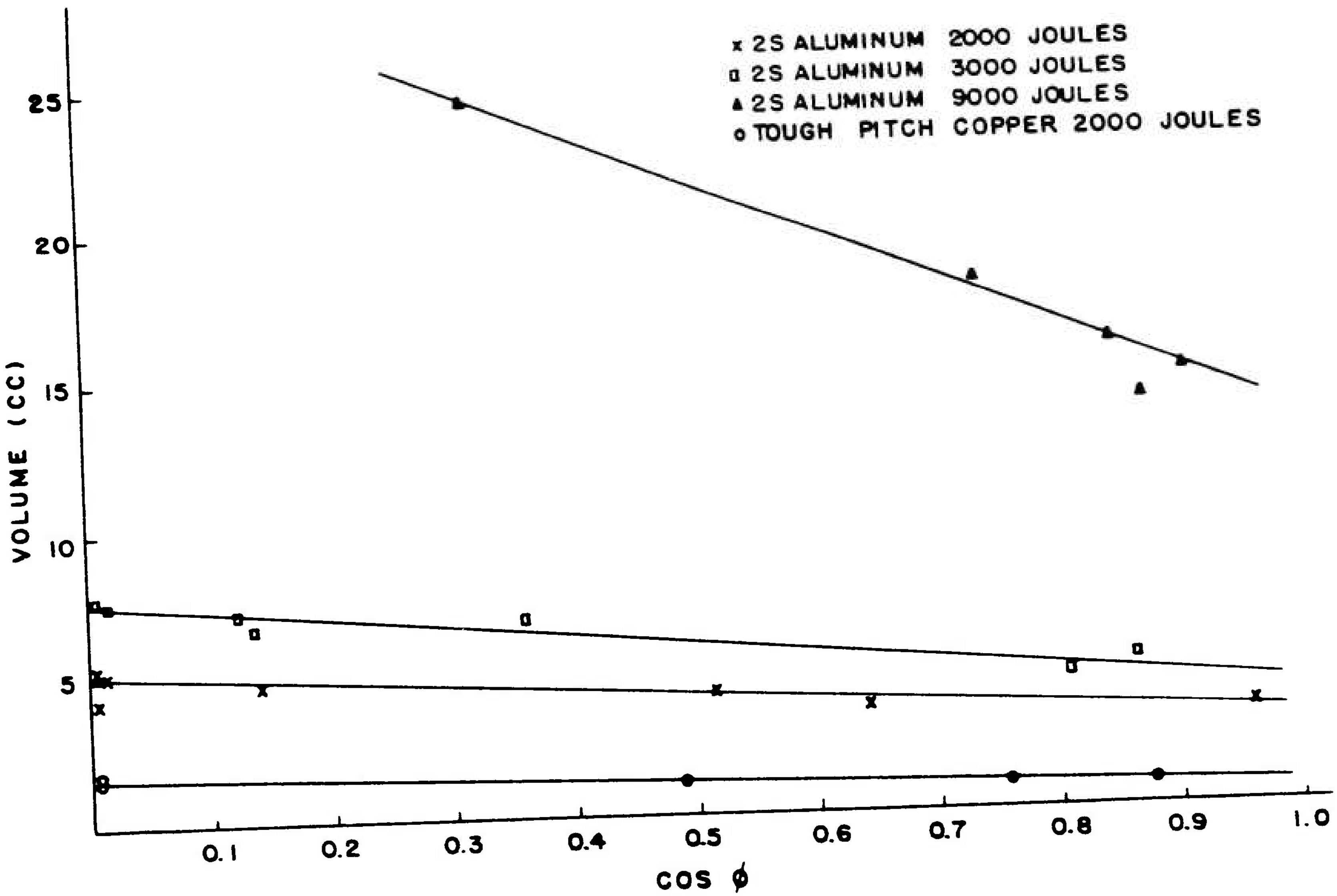

Fig. 8. Volume of Crater vs. Cosine of Orientation Angle, ϕ

ENERGY BALANCES ON 2S Al AIR GUN TARGETS

Energy balances have been completed for three of four 2S Al targets received from Technical Operations, Inc. These cylindrical specimens were impacted with a 6.06 mg mylar projectile traveling with an approximate velocity of 5×10^4 ft/sec. The fourth specimen was not analyzed since the projectile was breaking into two pieces at the time of impact.

Two of the targets were annealed in order to determine the variation of grain size as a function of strain. The energy balances were then carried out in the same manner as previously described (1).

The third target was analyzed using the hardness technique. Again, it was found that strain obeyed the expression:

$$\epsilon = e^{-\alpha(r-c)}$$

The results of the energy balances are as follows:

Specimen No.	Given Input Energy	Calculated Energy
3442	656.7 joules	82.5 joules
3444	690 joules	109.4 joules
3445	622 joules	152.8 joules

It was concluded that the input energies were probably in error due to an inaccurate value of velocity. Our results would tend to indicate that a velocity of approximately 2.0 to 2.5 $\times 10^4$ ft/sec would be more reasonable.

ENERGY BALANCES ON 2S Al WINDOWED TARGETS

Energy balances have been completed on five 2S Al windowed targets. Windowed targets are those having two parallel sides containing the direction of pellet travel. The parallel sides were machined on the sides of the 3 inch diameter cylinder target thereby reducing the minimum cross sectional value from 3 inches to 2 inches. The impact energy for these specimens was approximately 3,000 joules.

Hardness measurements were used to delineate strain as a function of the distance from the crater on the unannealed sectioned targets. After taking into account the average strain due to machining the target while being sectioned, curves which were approximately exponentially decaying were obtained. Therefore, we again use the equation

$$\epsilon = e^{-\alpha(r-c)}$$

The calculation of the energy terms was done in the same manner as for previous 2S Al cylindrical specimens. We did not take into account the change of geometry of the specimen. This is probably the reason why every energy balance completed was high. Also, it was noted that for this impact energy, the target was not semi-infinite. The energy balances were as follows:

Specimen Number	Impact Energy (Joules)	Calculated Energy (Joules)
40 W	3183.0	4052.9
41 W	3754.7	4537.0
45 W	2716.7	3268.2
45 W*	2716.7*	3648.2*
47 W	2658.5	4119.6
47 W*	2658.5*	2903.9*
50 W	2935.1	3353.3 4800.6

*Different analysis because of distinct variation in the value of α in $\epsilon = e^{-\alpha(r-c)}$

ENERGY BALANCES ON 2S Al PRE-STRAINED TARGETS

In the light of the energy balance technique the effect of prior cold working of 2S Al on its hypervelocity deformation behaviour was studied. Since cold working introduces strain energy in a metal, the strained metal should absorb less energy than is absorbed in the annealed state prior to rupturing. This decreased ability to absorb energy would infer a larger crater volume and/or strain affected region in comparison with hypervelocity penetration of the annealed metal. In effect, it was hypothesized that the energies of two deformation processes raising the strain level above the annealed state would be additive. The dynamic material properties governing the metal's behaviour would then be related to an annealed state by consideration of energy addition. Data indicate that this is <u>not</u> the case. The crater volume was smaller in the forged targets than that resulting from hypervelocity penetration of annealed 2S Al.

Seven cylindrical 2S Al annealed specimens were forged from approximately four inches in height to approximately three inches in height. The specimens were then machined on a lathe to dimensions of 3 inch height and 3 inch diameter. The specimens were then used as targets for the impact of hypervelocity projectiles of APG Charge Design No. 12.

The targets were sectioned through the center of the crater and polished so that Vickers Hardness (30 kg load) measurements could be made. The hardness measurements were analyzed and correlated to their corresponding strain values. Then, a plot of "Strain vs. Distance from Crater" was obtained. The "Strain versus Hardness

Measurement" curve for annealed 2S Al specimens was used in order to determine the "Strain vs. Distance" curve. The "Strain versus Distance" curve plotted on semi-log paper was quite different from any previous non-forged 2S Al specimens. Generally, there was a short length exponentially decreasing portion starting at the crater edge and extending approximately one centimeter. Following this portion there was a region of constant strain (generally of a value around 30%) which then decreased to some lower strain value at large distances from the crater (4 cm).

The specimens were analyzed by assuming that the constant strain level observed on the "Strain vs. Distance" curves was the average strain imposed on the specimen during forging. This strain value was subtracted from every strain value on the "Strain vs. Distance from Crater" curve in order to obtain the "Strain vs. Distance" graph for the hypervelocity impact. The resulting curve was exponentially decaying.

Energy balances were performed in the same manner as on any of the previous 2S Al specimens. The energy balances thus obtained are presented in Table 1. (Targets 101-107.)

From Tables 1 and 5 the crater volumes of forged targets are all less than the mean value of crater volumes in the annealed targets (1 through 10) penetrated by the same charge design (CD-12). The energy balances were not in agreement with the impact energy. The energy balance discrepancy is thought to result from the following:

1) Hardness measurements on the base of the fired targets were

extremely variable. This variation was probably introduced in the forging operation which also produced considerable "barreling" of the targets. This inhomogeneity carried over after the firing and made the strain affected region very difficult to analyze.

2) The dynamic rupture stress used in the energy balances was the value obtained for annealed aluminum. This had been felt to be justified on the hypothesis that dynamic rupture was dependent upon the metal's ability to absorb energy above some initial state and that energies absorbed would be additive in terms of producing rupture. On the basis of the crater volume data it appears that the material's dynamic strength properties have changed and that a different dynamic rupture stress should be considered.

Energy balances (Targets 104 and 105), see Table 1, were also computed using the strain field without correction for the initial deformation in forging. The estimated energy absorbed in forging was subtracted from the energy balance and the remainder ocmpared to the impact energy of hypervelocity deformation. The values listed in Table 1 are far too high to be reasonable. Comparison of these values, however, does not test the hypothesis about energy addition because of the uncertainty of the effect of cold working on the dynamic strength properties of the metal. We have been able to show only that, using the dynamic strength properties of the annealed metal, neither addition of the strain levels nor addition of the energies imposed in deformation leads to good energy balances.

The energy balances should be repeated with consideration given to the effect of cold working on strength properties before any conclusions are drawn.

NOMOGRAPHIC METHOD OF ENERGY BALANCE

To decrease the time required to perform the energy balances which involved extremely laborious arithmetic, a nomographical technique of energy balance was developed. A nomograph like the slide rule uses the addition and subtraction of lengths to represent the operations of normal arithmetic; however, a nomograph is set up to solve a specific equation for a certain range of variables rather than performing operations of multiplication and division (3).

First, it was found necessary to simplify the function for the energy of the strain affected region, E_{AR}. This expression may just as well be solved from the form

$$E_{AR} = \int_{r_0}^{r_m} \sigma_M \epsilon(r) \frac{dV_s}{dr} dr + \int_{r_0}^{r_m} \sigma_M \epsilon(r) \frac{dV_{cyl}}{dr} dr$$

where

V_s is the spherical portion of the strain affected volume

V_{cyl} is the cylindrical portion of the strain affected volume.

Evaluating this integral explicitly:

$$E_{AR} = k\left\{\epsilon_m\left[\left(r_0+\tfrac{1}{\alpha}\right)^2+\tfrac{1}{\alpha^2}\right] - \epsilon_0\left[\left(r_m+\tfrac{1}{\alpha}\right)^2+\tfrac{1}{\alpha^2}\right]\right\}$$

$$+ k'\left\{\epsilon_m\left(r_0+\tfrac{1}{\alpha}\right) - \epsilon_0\left(r_m+\tfrac{1}{\alpha}\right)\right\}$$

where $k = \frac{2\pi\sigma_m}{\alpha}$

$k' = kh$

The energy of the crater E_c is found by taking the product $\sigma_m \epsilon_m V_c$. This is actually in error by a term involving the elastic energy, but neglecting this term introduces an error much smaller than nomographic accuracy.

By nomographic techniques, a once laborious calculation has been reduced to a 10 minute procedure. The nomographic method gives answers within slide rule accuracy. Copies of the nomographs and instruction for use can be procured upon request from the authors.

ENERGY BALANCES ON STATICALLY DEFORMED TARGETS

In order to examine the validity of the energy balance technique used on hypervelocity targets, analogous energy balances were performed on statically deformed 2S Al targets and on a 2S Al and two mild steel tensile specimens. Evidence of the validity of scaling the strains derived from hardness measurements on dynamically deformed material was provided. This evidence came from the essential linearity in the plastic region of energy/volume vs. strain in the tensile specimens. The necessity for further investigation to determine the nature of the consistent difference between mechanical work as defined from a load deflection curve and plastic work defined by the material stress-strain curve is suggested by the results presented. Understanding the difference between the dynamic and static cases may lead to a better understanding of concepts such as stored energy of cold-work. The consistent difference between input energy as calculated from a load deflection curve and the energy balance from a stress-strain curve (static) is troublesome, since the data indicate that the total input energy as defined cannot be accounted for from considerations of the plastic work expression

$$E = \int_V \left[\int \sigma \, d\epsilon\right] dV$$

Static energy balances were effected for four 2S Al annealed specimens. Using the Universal Testing Machine, 1/2 inch diameter steel ball-bearings were impressed on three cylindrical specimens at the rate of 0.00165 inch/second. A 1/4 inch diameter steel ball-bearing was impressed on the fourth specimen at the same rate. The area under the measured "Load-Deflection" curve was used as the input energy for each specimen. The specimens were then sectioned in half through the center and polished so that Vickers Hardness measurements could be made. The hardness measurements, as a function of distance from the approximately hemispherical crater, were used to obtain a "Strain versus Distance from Crater" curve for the particular specimen. It was found, as in the hypervelocity targets, that strain could be expressed as a function of the radial distance from the crater center by the formula

$$\epsilon = e^{-\alpha(r-c)}$$

where α and c are constants determined from physical measurements. (See Reference (1).)

In order to evaluate the energy in the specimens it was necessary to know stress as a function of strain for 2S Al specimens tested at standard rates. The stress-strain curves of two standard tensile specimens (2S Al No. 15 and 2S Al No. 16) were used. These stress-strain curves were closely approximated by two straight lines. Thus,

$\sigma = A_1\epsilon + B_1$ (From 0.00 in./in. strain to 0.05 in./in. strain)

and

$\sigma = A_2\epsilon + B_2$ (From 0.05 in./in. strain to 0.735 in./in. strain)

The average values of the coefficients were found to be the following:

A_1	= 111,000 psi	B_1	= 4,100 psi
A_2	= 26,277.4 psi	B_2	= 8,286.1 psi

Using this information, it was possible to calculate the energy from the formula,

$$E = \int_{r_o}^{r} \left[\int \sigma(\epsilon) d\epsilon \right] \left[\frac{dV}{dr} \right] dr$$

For our particular problem,

$$E = \pi A_2 \left[\left(\frac{r_o^2}{2\alpha} + \frac{r_o}{4\alpha^2} + \frac{2}{8\alpha^2} \right) \epsilon_M^2 \right] + \pi (A_1 - A_2) \left[\left(\frac{r_y^2}{2\alpha} + \frac{r_y}{4\alpha^2} + \frac{2}{8\alpha^3} \right) \epsilon_y^2 \right]$$

$$+ 2\pi B_2 \left[\left(\frac{r_o^2}{\alpha} + \frac{2 r_o}{\alpha^2} + \frac{2}{\alpha^3} \right) \epsilon_M \right] + 2\pi (B_1 - B_2) \left[\left(\frac{r_y^2}{\alpha} + \frac{2 r_y}{\alpha^2} + \frac{2}{\alpha^3} \right) \epsilon_y^2 \right]$$

$$- \pi A_1 \left[\left(\frac{r_m^2}{2\alpha^2} + \frac{r_m}{4\alpha^2} + \frac{2}{8''} \right) \epsilon_o^2 \right] - 2\pi B_1 \left[\left(\frac{r_m^2}{\alpha} + \frac{2 r_m}{\alpha^2} + \frac{2}{\alpha^3} \right) \epsilon_o \right]$$

$$- \pi (\epsilon_y - \epsilon_o)(B_2 - B_1) \left[r_y^3 - r_o^3 \right]$$

r_o is the radius of the crater formed; r_y is the radius measured from the center of the crater, corresponding to the strain ϵ_y. ϵ_y equals a strain of 0.05 in./in. in our problem. r_m is the radius corresponding to the strain ϵ_o = 0.01 in./in.

Using the measured values for these parameters energy balances were obtained as shown on Table 6.

Note: While effecting these static energy balances, it was shown that hardness measurements could be used to determine the effective strain placed in the surface layer (a thin volume element) of a specimen during machining. For the relatively soft 2S Al specimens, it was found that machining on a lathe (with light cuts) and/or polishing on a coarse belt produced 2.5 to 3.0 per cent strains in the surface layers. These strains, due to machining, had to be subtracted from the measured strains in order to obtain the correct strain resulting from the deformation in question.

TABLE 6

STATIC ENERGY BALANCE

2S Al

Specimen No.	Energy Input Ft.-Lb.	ϵ_m	ϵ_y	ϵ_o	r_o in.	r_y in.	r_m in.	α in^{-1}	E_{AH} ft.-lb.	$\frac{E_{AR}}{E_I}$ %
39	102.89	0.66	0.05	0.01	0.2435	0.6055	0.8325	7.113	69.42	67.47
40	118.27	0.68	0.05	0.01	0.2465	0.6065	0.8265	7.275	70.68	59.76
43	198.00	0.82	0.05	0.01	0.25	0.7224	0.9902	5.9521	145.2	73.33
44	22.38	0.75	0.05	0.01	0.125	0.3219	0.4321	14.059	12.05	53.84

The A, B, A' and B' values for all specimens are the same, as follows:

$A = 26,277 \ lb/in^2$

$B = 8,286 \ lb/in^2$

$A' = 110,000 \ lb/in^2$

$B' = 4,100 \ lb/in^2$

STATIC ENERGY BALANCES ON STANDARD TENSILE SPECIMENS

Energy balances were performed on two standard 1014 steel tensile specimens. The standard tensile specimens were machined to specification and then annealed (brought to 1650°F., held for five minutes, then furnace cooled).

Using the Universal Testing Machine, the specimens were deformed in tension until rupture. During the tension tests the loads, deflections (across a two inch gauge) and diameters were recorded.

The areas under the "Load-Deflection" curves were used as input energies. From the true stress - true strain curves modified as previously report (1), a graph of "Energy per Unit Volume versus Strain" was constructed. The two specimens were then mounted and sectioned in half parallel to the tensile axis. Vickers Hardness measurements were made along the specimen and analysed so that strain, as a function of distance from gauge mark (or rim), could be determined. Then, knowing the strain at each length interval of the specimen and measuring the cross sectional area of each interval of length, it was possible to obtain the energy in each such interval. The total energy was the summation of energies of each interval. This total energy was compared to the input energy.

The following balances were obtained:

Specimen No.	Input Energy	Measured Energy
1	8,400 in-lb	6,078 in-lb
2	9,100 in-lb	7,026 in-lb

A similar static energy balance was done on a 2S Al tensile specimen. The results were as follows:

Specimen No.	Input Energy	Measured Energy
20	1,944 in-lb	1,145 in-lb

From the plot in Fig. 9 of energy/volume vs. strain it is found that in the tensile specimens there is virtually a linear relation between these quantities. A linear relation (with a different slope) is postulated in hypervelocity for deformation between energy/volume and strain, Fig. 9. This indicates that the error in scaling up the strains in dynamic deformation determined from correlation with hardness measurements on statically deformed specimens is negligible. That is since the ratio of dynamic energy/volume to static energy/volume is essentially a constant for all strains, then it is permissible to multiply strains determined on the targets from static strain vs. hardness plots by a constant in order to obtain the dynamic balances.

Static energy balances by the above method have proven consistently low, accounting for only 60 - 70% of the work done on the test pieces computed from the load-deflection curve. The energy which can be accounted for is taken as that value calculated from the usual expression for the energy associated with plastic work:

$$E = \int_V \left[\int \sigma \, d\epsilon \right] dV$$

The difference in the values from the two definitions of energy is consistent enough that the choice of one as being more meaningful than the other is not felt to be well founded a priori to an experimental determination (via calorimetric studies) of heat evolved during the deformation of metals. On the other hand, whichever definition of energy is chosen, it is felt that the other is related to it in a predictable and explicable manner.

Two questions raised are not answerable at this time:

1. Why is the difference between the energies so consistent and will this consistency carry over to the hypervelocity case?
2. What fraction of the work done is actually residual strain energy and what fraction is heat or other dissipative loss?

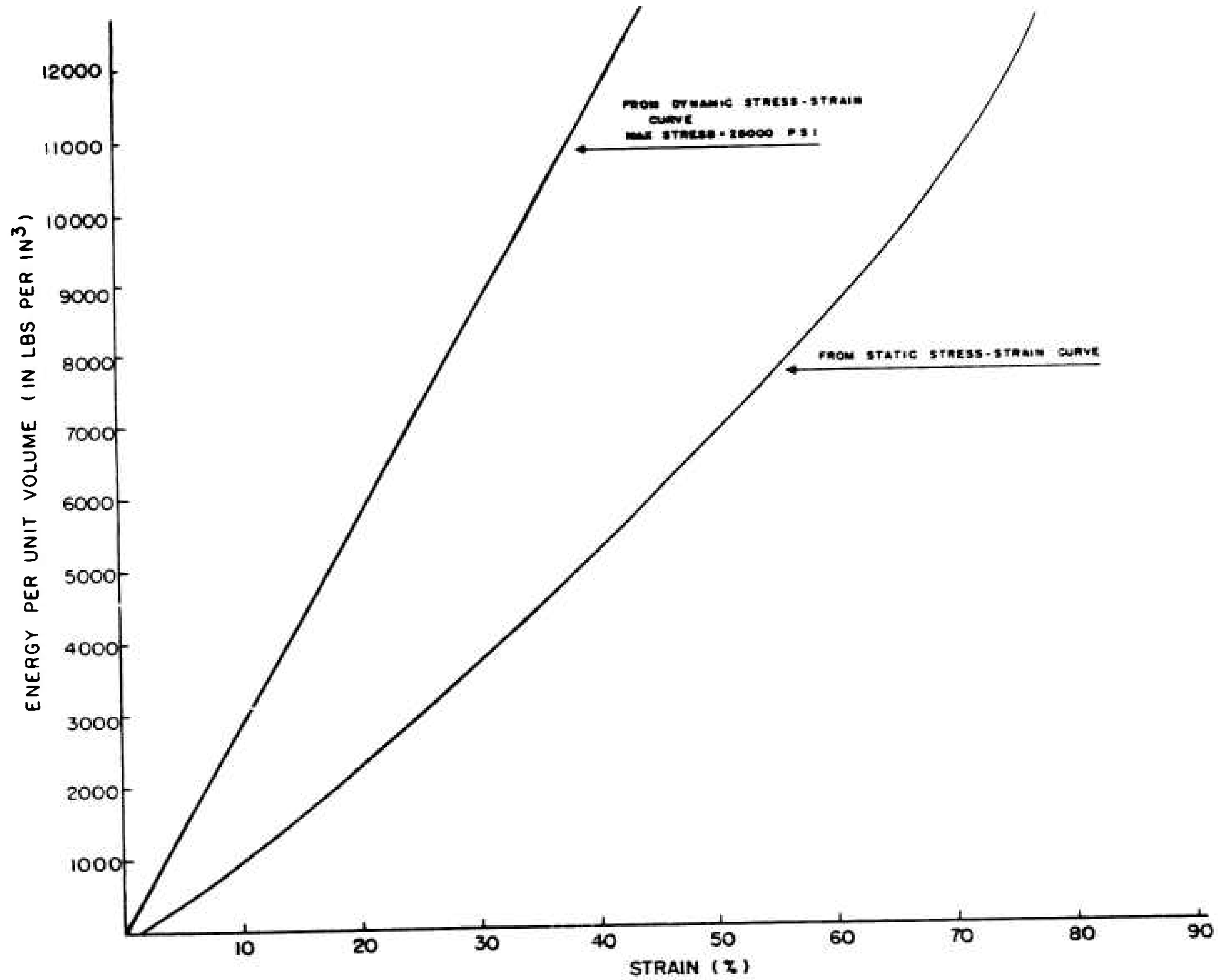

Fig. 9. Energy/Volume vs. Strain in 2S Al - from Static and Dynamic Curves

STRENGTH PARAMETERS RELATED TO THE PARTITION OF ENERGY

It was stated in a previous report (1) that as the crater takes on an appreciable size, the ratio of the crater volume to the strain affected volume rapidly approaches a constant value in 2S Al of .15. While the energy associated with these respective volumes is not in the same ratio, it is possible to calculate it from energy balances at the 2000 Joule level of impact energy in Cu and 2S Al and to predict this ratio from considerations independent of the energy balances. The observed correlation of these independent derivations of the ratios of crater energy to major strain affected region energy gives some evidence of the validity of the energy balance technique. The aforementioned ratio is shown to be given in terms of parameters already known and which are properties of the target and projectile materials at hypervelocity.

For the purposes of this discussion Cu and 2S Al at 2000 Joules impact energy are investigated for the reason that at this energy the targets have been of sufficient size to account for the impact energy as having been dissipated in the formation of the crater, the high strain region associated with the material adjacent to the crater, and the low strains in the remainder of the specimen. In other words our energy balance technique is able to account for the energy of impact as being dissipated primarily through deformation of the specimen.

In performing energy balances the energy of crater formation was represented by the amount of energy required to raise the material which once occupied the crater to rupture stress and rupture strain on the presumed hypervelocity stress-strain curve. The energy/volume necessary to do this is the rupture stress x rupture strain less a small term for elastic energy. This product is denoted as K. Let E_c be the energy of crater formation; then 1) $E_c = KV_c$, where V_c is the crater volume.

Empirical observations made on the relationship of crater volume as a function of the impact energy re-emphasize the often made point that there is a linear relationship between these two quantities at the velocities which were studied. If we plot crater volume vs. impact energy and denote the slope of this straight line which passes through the origin by M; then we may say that:

2) $V_c = ME_I$, where E_I is the impact energy.

Since our energy balances infer that the energy of impact may be accounted for by the energies of crater formation and strained regions we may write:

3) $E_I = E_c + E_{AR}$

or

4) $E_I - E_c = E_{AR}$

where E_{AR} is the energy associated with deformation adjacent to the crater.

E_{AR} is calculated from the energy balance technique previously described. The ratio of the crater energy to the energy of the deformation of the remainder of the material is obviously $\frac{E_c}{E_{AR}}$.

Noting that from 4) $E_{AR} = E_I - E_o$, then $\frac{E_o}{E_{AR}} = \frac{E_o}{E_I - E_o}$.

From relations 1) and 2) we may solve for the ratio $\frac{E_o}{E_I - E_o}$ in terms of the material constants K and M. Doing this we find

$$\frac{E_o}{E_I - E_o} = \frac{KM}{1 - KM}$$

or

$$\frac{E_o}{E_{AR}} = \frac{KM}{1 - KM}$$

Since K and M are material constants, it is possible to determine the partitioning of the energy between the crater and remaining deformed material in terms of strength properties. These properties are derivable independent of the energy balances. K is a dynamic modulus of toughness of the target and M is the slope of V_o vs. E_I and is dependent upon the material of the target and projectile.

Table 7 gives a comparison of average values of $\frac{E_o}{E_{AR}}$ and $\frac{KM}{1 - KM}$ for 2S Al, Cu and 1014 steel targets tested at 2000 Joules.

The agreement of these independently determined ratios gives evidence that our energy balance is consistent with other experimental observations. A parameter $\frac{KM}{1 - KM}$ is presented which may be useful in evaluating the relative behaviour of materials in terms of energy absorption at hypervelocity. In the energy range tested, K is specifically a constant of the target material. M is a constant of the target and projectile materials. The energy partition parameter will depend only on these variables so long as the target is of sufficient size to absorb all of the impact energy.

Finally, it should be noted that the velocity ranges tested here are from 3 - 5 km/sec and are such that the use of strength properties of the material in evaluation of energy dissipation in the target seems justified (4,5).

TABLE 7

Material	Joules/cc K	cc/Joule x 10^{-4} M	Avg. (Joules) E_c	Avg. (Joules) E_{AR}	$\frac{E_c}{E_{AR}}$	$\frac{KM}{1 - KM}$
Cu	187.5	6.16	234.6	1627	.144	.131
2S Al	139.4	20.6	606.2	1400	.433	.403
1014 Steel Targets 3-7 Best values of E_T	728.3	3.25	500.6	1208.6	.414	.340

GENERAL DISCUSSION

The evidence of the validity of the energy balance technique must be based upon the results it obtains. Agreement with impact energy is very good in instances where the major deformation is confined within the targets, that is where gross deformation (bulging of the sides, e.g.,) did not occur. However, for the 3 in. x 3 in. cylindrical targets at 9000 Joules impact energy considerable bulging does occur. This same effect occurs to an even greater extent in the window targets. For these cases the energy balances were not good.

Strength parameters have been shown to play a role in hypervelocity deformation at the velocities and energies tested. Yet the energy balances per se have been couched in certain assumptions about the hypervelocity behaviour of metals. Independent experiments must be made to verify or discredit these assumptions.

The hypothesized stress-strain curve implies that deformation proceeds at a constant level of stress with a strain hardening index of 0. Hardness measurements below craters in the targets indicate that there is an increase of hardness. This would contradict the above assumption unless it can be shown that a delay time for strain hardening does exist. This would allow deformation to occur and then to be followed by hardening.

To correlate dynamic strains with a static strain vs. hardness plot the hardness level at a given strain was assumed to be a function of strain rate as well as the level of strain. Some indication of this scaling of strain values is mentioned in the section on

Static Energy Balances. The evidence is not direct and further study is necessary on this aspect of the energy balance technique.

Correlation of volume with pellet orientation at impingement has been made. Indications are that the pellet orientation affects the energy balance, but the nature of this variation in terms of parameters, such as α, has not been established. Work with forged targets, statically loaded standard tensiles and statically impressed targets has opened questions concerning the nature of the energy absorbed in deformation of metals. These questions are of a fundamental nature and involve an investigation of definitions of work by a load deflection curve as opposed to a definition of plastic work by the the expression:

$$\int_{Volume} \left\{ \int \sigma \, d\epsilon \right\} dV$$

Another question concerns the partitioning of the work done in any deformation between heat energy and/or other losses and the energy which remains latent in the specimen. This residual energy of cold-work may be related to the increase of dynamic strength properties and thereby shed light on the behaviour of the forged targets.

Bibliography

1. R. B. Pond, C. Mobley and C. M. Glass, "Energy Balances in Hypervelocity Penetration," _Proceedings of the Sixth Symposium on Hypervelocity Impact_, Volume 11, Part 2, (1963) 401 - 417.

2. C. M. Glass and R. B. Pond, "A Metallurgical Approach to the Hypervelocity Problem," _Proceedings of Fourth Symposium on Hypervelocity Impact_, Volume 111 (1960)

3. Lee H. Johnson, _Nomography and Empirical Equations_, John Wiley & Sons, Inc., New York, 1952.

4. R. L. Bjork, "Review of Physical Processes in Hypervelocity Impact and Penetration," _Proceedings of the Sixth Symposium on Hypervelocity Impact_, Volume 11, Part 1, (1963), 29-31

5. J. H. Kineke, Jr., and L. G. Richards, "Influence of Target Strength on Hypervelocity Crater Formation in Aluminum," _Proceedings of the Sixth Symposium on Hypervelocity_, Vol. II, Part 2 (1963), pg. 517-519.

U. S. Army Materiel Command
ATTN: Mr. Mel C. Miller
Washington 25, D. C.

U. S. Army Material Command
ATTN: Dr. Peter Kasting
Washington 25, D. C.

Army Materials Research Agency
Watertown Arsenal
ATTN: Paul Riffin
Watertown 72, Mass.

Army Materials Research Agency
Watertown Arsenal
ATTN: Melvin P. Marks
Watertown 72, Mass.

Army Materials Research Agency
Watertown Arsenal
ATTN: B. Goldberg
Watertown 72, Mass.

National Bureau of Standards
ATTN: L. L. Wyman
Washington, D. C.

Director of Defense Research & Eng.
(OSD)
Washington 25, D. C.

Naval Research Laboratories
ATTN: Dr. Floyd B. Brown
Washington 25, D. C.

Army Research Office
Box CM, Duke Station
ATTN: Joseph R. Lane
Durham, North Carolina

Army Research Office
Box CM, Duke Station
ATTN: Franz K. Wedeling
Durham, North Carolina

Commanding General
Frankford Arsenal
ATTN: Harold Marcus
Philadelphia 37, Pennsylvania

Commanding Officer
Picatinny Arsenal
ATTN: Mr. James Killen
Dover, New Jersey

U. S. Army Ordnance Missile Command
ATTN: Dr. Bernard Steverding
Redstone Arsenal, Alabama

U.S. Atomic Energy Commission
ATTN: Technical Reports Library
Washington 25, D. C.

Naval Research Laboratories
ATTN: J. M. Krafft
Washington 25, D. C.

Air Force Special Weapons Center
ATTN: Capt. Donald Lamberson
Kirtland Air Force Base, N. M.

Wright Air Development Division
Wright-Patterson Air Force Base
ATTN: Mr. Alan Hopkins, ASCPR
Dayton, Ohio

Chief of Research & Development
Department of the Army
ATTN: Army Research Office
Washington 25, D. C.

Library of Congress
Technical Information Division
Reference Department
ATTN: Bibliography Section
Washington 25, D. C.

U. S. Army Chemical Warfare Labs.
ATTN: Dr. B. Harris
Edgewood Arsenal
Maryland

U.S. Naval Weapons Evaluation Facility
ATTN: Jack Abbott, Code 3434
Kirtland Air Force Base
New Mexico

U. S. Naval Weapons Laboratory
ATTN: Dr. William Soper
Dahlgren, Virginia

U. S. Dept. of Interior
Bureau of Mines
ATTN: Mr. R. Watson
4800 Forbes Street
Pittsburgh 13
Pennsylvania

Director
NASA
Lewis Research Center
21000 Brookpark Road
Cleveland 35, Ohio

Director
NASA
Ames Research Center
Moffet Field, California

Commanding Officer
Watervliet Arsenal
ATTN: Fred Schniedeshoff
Troy, New York

Commanding General
ATTN: Mr. Walter H. Dettrich
Det. 4 ASD, ASQWR
Eglin Air Force Base, Florida

Commanding Officer
Army Research Office
Material & Chemistry Division
Arlington Hall Station
Arlington 12, Virginia

Advanced Research Projects Agency
ATTN: Capt. R. B. Greenwood
Washington 25, D. C.

Dr. Hoyt Andersen
Aerojet General Corporation
11711 S. Woodruff Avenue
Downey, California

Mr. Edward Custerer
Aircraft Armaments, Inc.
York Road
Cockeysville, Maryland

Dr. Conrad Bruenner
Boeing Scientific Research Lab.
Boeing Airplane Co.
P. O. Box 3707
Seattle 24, Washington

Mr. Stan W. Porembka
Battelle Memorial Institute
505 King Avenue
Columbus 1, Ohio

Mr. Milton Cox
Firestone Tire & Rubber Co.
Defense Research Division
Akron, Ohio

Mr. V. F. Zackay
Ford Motor Co.
2000 Rotunda Drive
Dearborn, Michigan

Mr. C. R. Cassity
General Electric Co.
Huntsville, Alabama

Dr. A. M. Bueche
General Electric Co.
Aeroscience Laboratory
3750 D. Street
Philadelphia, Pennsylvania

Dr. E. G. Zukas
Los Alamos Scientific Laboratory
Los Alamos, New Mexico

Dr. Max Solow
Martin-Marietta Co.
Baltimore 20, Maryland

Dr. Irvin Kramer
Martin-Marietta Co.
Baltimore 20, Maryland

Dr. D. Toner
Oak Ridge National Laboratory
Metallurgical Division
P. O. Box X
Oak Ridge, Tennessee

Stamford Research Institute
Poulter Laboratories
Menlo Park, California

Mr. J. W. Gehring
General Motors Corp.
Flight Physics Lab.
Box T
Santa Barbara, California

Dr. J. E. Dorn
University of California
Berkeley, California

Dr. Roy B. Noyes
University of California
Lawrence Radiation Laboratory
Livermore, California

Prof. Paul Shewmon
Carnegie Institute of Technology
Schenley Park
Pittsburgh 13, Pennsylvania

Dr. John S. Rinehart
Colorado School of Mines
12 Mines Road
Golden, Colorado

Dr. George Dieter
Drexel Institute of Technology
Philadelphia 4, Pennsylvania

Dr. Louis Teutonico
Republic Aviation Corp.
223 Jericho Turnpike
Mineola, Long Island
New York

Mr. Donald C. Lundergan
Sandia Corporation
Sandia Base
Albuquerque, New Mexico

Dr. D. C. Drucker
Brown University
Providence, Rhode Island

Dr. H. Kolsky
Brown University
Providence, Rhode Island

Dr. D. S. Wood
California Institute of Technology
Division of Engineering
Pasadena, California

Mr. R. Recht
Denver Research Institute
Mechanics Division
University of Denver
Denver 10, Colorado

Dr. W. Rostocker
Armour Research Foundation
10 West 35th Street
Chicago 16, Illinois

Dr. Walter Hermann
Massachusetts Institute of Technology
Cambridge 39, Mass.

Dr. Johannes Weertman
Northwestern University
Material Science Department
Evanston, Illinois

Commanding Officer
U.S. Army Ordnance District,
Philadelphia
128 N. Broad Street
Philadelphia 2, Pa.
ATTN: OD, R&D Branch (3)

Commanding General
U. S. Army Proving Ground,
Aberdeen
Maryland
ATTN: Director, BRL

Commander
ASTIA, Arlington Hall Station
Arlington 12, Virginia
ATTN: TIPDR (10)

Commanding Officer
Diamond Ordnance Fuze Labs
Washington 25, D.C.
ATTN: Tech. Reference Section
ORDTL 06.33

Defense Metals Info. Center
Battelle Memorial Institute
505 King Street
Columbus, Ohio

Battelle Memorial Institute
505 King Avenue
Columbus 1, Ohio
ATTN: Battelle-DEFENDER

Battelle Memorial Institute
505 King Avenue
Columbus, Ohio 43201
ATTN: Reports Library (GID)

Scientific and Technical Info.
Facility
ATTN: NASA Representative (S-AK/DL)
P. O. Box 5700
Bethesda, Maryland

Professor John Zotos
Dept. of Mechanical Eng.
Northeastern University
360 Huntington Ave.
Boston 15, Massachusetts

Dr. L. E. Malvern
Michigan State University
East Lansing, Michigan

Dr. Norman Brown
University of Pennsylvania
Department of Metallurgy
Philadelphia 4, Pa.

Dr. Gordon Filbey
University of Pennsylvania
Mechanics Department
Philadelphia 4, Pennsylvania

Dr. E. H. Lee
Stanford University
Palo Alto, California